Int. J. Electrochem. Sci., 14 **(2019)** 10032 – 10042, doi: 10.20964/2019.11.19

International Journal of
ELECTROCHEMICAL
SCIENCE
www.electrochemsci.org

Effect of Thermal Conditions on Corrosion Behavior of Ductile Cast Iron

Chien-Hung Lin[1*], *Jia-Ren Lee*[2], *Pei-Jing Teng*[1]

[1] Department of Physics, ROC Military Academy, Feng-Shan, Kaohsiung, Taiwan
[2] Department of Physics, National Kaohsiung Normal University, Kaohsiung, Taiwan
[*]E-mail: linhungcma@gmail.com

Received: 2 July 2019 / *Accepted:* 21 August 2019 / *Published:* 7 October 2019

Spherical nodules inhibit crack propagation in ductile cast iron (DCI) and improve its ductility. In this study, we investigated the failure mechanism of DCI under atmospheric exposure and carried out slow strain rate testing (SSRT) to evaluate its mechanical properties. The tensile strengths of the DCI specimens at the operational temperatures of −30 and 100 °C were 440.2 and 388.8 MPa, respectively. The mechanical strength of the DCI specimens decreased with an increase in the operational temperature. Moreover, the corrosion current densities of the DCI specimens in the presence of brine water at 100 and 27 °C were 3.84×10^{-4} and 3.97×10^{-5} A/cm^2, respectively. Under ambient conditions, the corrosion rate of DCI was more than one order of magnitude lower than that under the extreme condition. The DCI specimens exhibited poor mechanical performance in the presence of brine water (3.5 wt% NaCl), especially in boiled water because of their stress corrosion cracking. Consequently, the DCI specimens showed partial ductile fracture because of their quasi-cleavage features in the ambient environment and brittle-type cleavage fracture in brine water. The microscopic observations were consistent with the SSRT results. The findings of this study will be helpful in improving the mechanical properties of DCI.

Keyword: ductile cast iron, slow strain rate testing, stress corrosion cracking, ductile

1. INTRODUCTION

Cast iron consists of carbon (more than 2%) and iron. Cast iron is extensively used in industrial pipes owing to its excellent machinability, castability, wear-resistance, and hardness. Ductile cast iron (DCI) show better ductility than cast iron because of the presence of spherical nodules in it. Hence, ductile iron pipes are widely used in pipeline engineering. Pipeline transportation is extensively used to transport water, crude oil, sewage, fuel gas, and chemical liquids. The major advantages of pipeline transport are its high speed and safety (for long distances). Pipelines should possess a pressure pipe, large diameter, and environmental resistance for transmission. In addition, the huge industrial demand

for transportation of various commodities led to the development of pipelines. Various studies have been carried out to investigate the fundamental properties of cast iron [1-3].

In a previous study, the SCC (stress corrosion cracking) of spheroidal graphite cast iron in caustic environments was investigated [4]. It was found that cracks originate at the grain boundary pit and their intergranular propagation occurs through ferrite boundaries. The external force: stress ratio ($R = K_{min}/K_{max} = 0.1; 0.5; 0.75$) was varied to discuss the fatigue behavior of DCI. It was found that different microstructures of ductile iron are susceptible to the austempering treatment process. All the specimens consisted of various proportions of the ferrite and pearlite phases. The results demonstrated that the fatigue crack propagation resistance of the DCI specimens was affected by the de-bonding of graphite elements. Furthermore, in another study, ductile iron was characterized to determine the graphite element location. It was found that the crack propagation predominantly depended on the mechanical behavior of the ferrite and pearlite phases [5]. Nickel (> 4%) is considered as an austenite stabilizer, and the pearlite content of DCI increases with an increase in the number of nodules in the matrix microstructure [6]. Meanwhile, the corrosive resistance of nickel-alloyed ductile iron improves with tempering even in the presence of sodium chloride (3.5% wt NaCl).

The impact energy and tensile strength properties of DCI depend on the ferritic and pearlitic matrix proportions, respectively. The mechanical properties of heat-treated DCI were evaluated by carrying out its tensile and impact tests [7]. The fractography results revealed the occurrence of graphite longitudinal deformation in the DCI matrix. It was demonstrated that austempering improved the strength of DCI because of the presence of a bull's-eye structure around its ferritic phase. Moreover, transgranular propagation through ferritic grains in DCI occurs because of its plastic behavior. Low-temperature impact testing has been employed to investigate the toughness of nickel-alloyed DCI [8]. After the annealing treatment, the pearlite phase exists in the matrix microstructure, and the corrosion rate of DCI decreases with an increase in the nickel content (0–1.8 wt%) in brine water (3.5 wt% NaCl). However, the coexistence of the pearlite and cementite phases deteriorates the toughness of nickel-alloyed DCI.

DCI with 0.71 wt% nickel shows excellent toughness in a subfreezing environment (−40 °C). The effects of environmental parameters (NaCl concentration, pH value, operational temperature) on the failure mechanism of DCI have also been investigated in a circulating water tank [9]. The corrosion potential of DCI decreases with an increase in the NaCl concentration. In addition, the corrosion rate of DCI increases with an increase in the operational temperature, particularly in the waterline zone.

While many reports are available on DCI, only a few of them have focused on its SCC behavior. Hence, the objective of this study was to investigate the SCC behavior of DCI in the presence of brine water. Slow strain rate testing (SSRT) under hyperthermal conditions caused brittle failure in DCI. Improving the mechanical performance of DCI in brine water is crucial for realizing its practical applications.

2. EXPERIMENTS

2.1. Metallographic analysis

DCI was used as the raw material in this study, and its composition (wt%) is listed in

Table 1. The gauge area was 2.5 mm-thick and the dimensions of the processed specimens are shown in Fig. 1. The tensile specimens were machined according to ASTM E8 standard.

Table 1. Chemical composition of DCI.

Element	C	Si	Mn	P	Mg	S
weight%	3.18	2.58	0.18	0.035	0.5	0.005

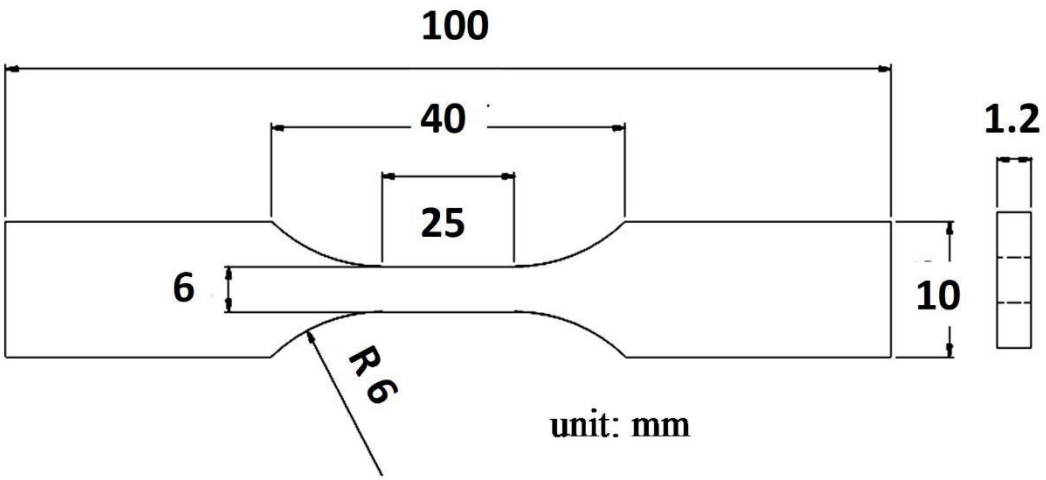

Figure 1. Tensile dimensions of the DCI specimens (ASTM E8 standard).

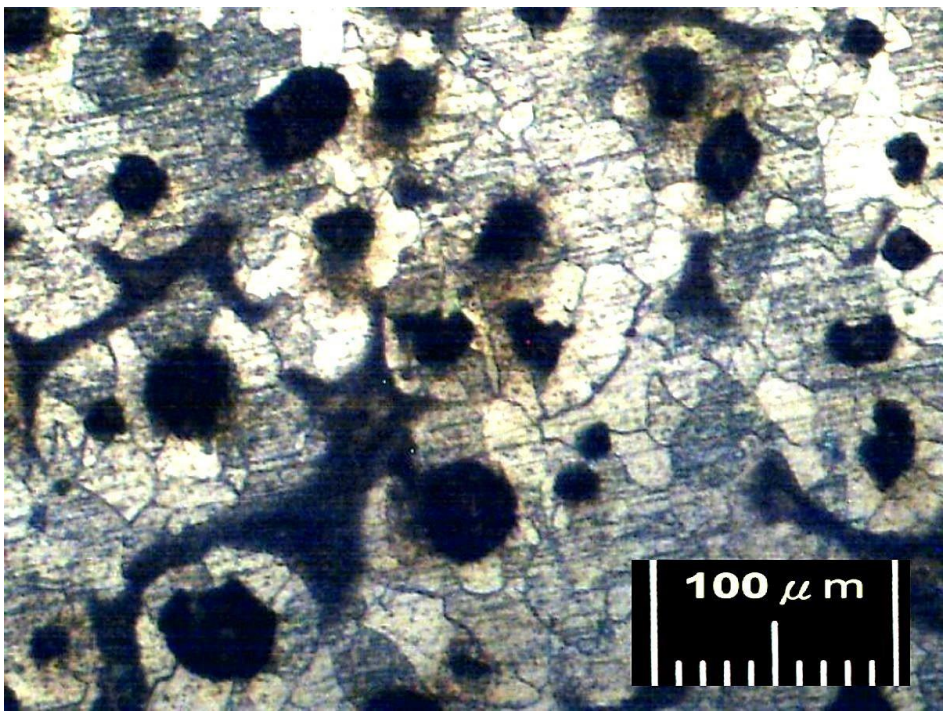

Figure 2. Metallographic image of DCI.

The surface of every specimen was ground with 800# grit emery paper, then degreased with acetone to reduce the artificial defects on its surface. Prior to SSRT, the specimens were dehydrated under a stream of hot air (65 °C) for 1 h. In the DCI specimens, the graphite element appeared as spherical nodules and was embedded in the matrix. The metallographic structure shown in Fig. 2 reveals the co-existence of graphite, pearlite, and ferrite grains at the surface of the specimens. The graphite nodularity and size of the ferrite grains were found to be approximately 80% and 50 μm, respectively.

2.2. Constant strain-rate experiment

SSRT was carried out in atmospheric and brine environments (3.5 wt% NaCl) at five different temperatures: 100, 70, 27, −10, and −30 °C. The strength, elongation rate, and stress strain curves of the specimens were obtained at the tensile strain rate of $2.5 \times 10^{-5} sec^{-1}$.

2.3. Electrochemical measurements

Electrochemical measurements were carried out in a corrosive aqueous environment (3.5 wt% NaCl). Potentiodynamic and open circuit potential (OCP) techniques were employed to investigate the corrosive resistance of DCI in brine water. The gauge dimensions (1 cm^2) of the specimens were electrochemically monitored using a Versastat 4 system (AMETEK Inc). A standard three-electrode system with the specimen as the working electrode, a Ag/AgCl electrode as the reference electrode, and a platinum electrode as the auxiliary electrode was used. The polarization curves obtained from the potentiodynamic measurements of the specimens were used determine their corrosive potential and current. As the potentiodynamic test, the sweeping potential and scan rate were 0.2 to −1.1 Volt and 0.5 mV/s, respectively. Furthermore, the stability of the oxide film on the DCI surface was investigated using the OCP methodology for 5000 s.

3. RESULTS AND DISCUSSION

3.1. Mechanical properties

The elongation rates and tensile strengths of the specimens treated at various temperatures are shown in Fig. 3. It can be observed from the figure that the strength of DCI was significantly affected by the thermal processing conditions. The specimens treated at 100 and 27 °C showed tensile strengths of 388.8 and 408.5 MPa, respectively. The strength of the specimens decreased with an increase in the operational temperature (Table 2).

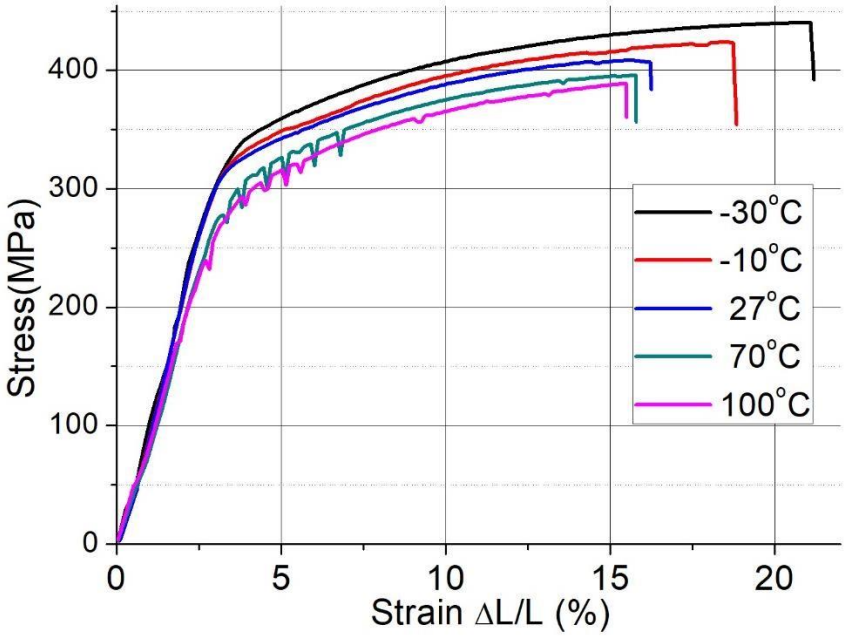

Figure 3. Tensile stress-strain curves of DCI exposed to atmospheric environment (strain rate 2.5 x $10^{-5}$$sec^{-1}$).

Table 2. Tensile properties of the DCI specimens exposed to brine water at various temperatures.

Condition	Temperature	Ultimate tensile strength (MPa)	Strain (%)	Failure time (hour)
Atmospheric	100℃	388.8	15.4	103
	70℃	395.6	15.7	105
	27℃	408.5	16.2	108
	-10℃	423.6	18.8	125
	-30℃	440.2	21.1	141
Brine water	100℃	294.6	7.8	52
	70℃	305.7	9.9	66
	27℃	385.5	14.5	97

The highest strength was obtained at the subfreezing temperature (−30 °C). This indicates that the microcracks propagated slowly and a large amount of energy was absorbed during the plastic deformation at low temperatures. However, void nucleation, crack propagation, and dislocation movement were observed at low temperatures. The accumulation and coalescence of vacancies promoted

the propagation of micro-cracks until the occurrence of fracture [10]. The segregation of the interstitial impurity (carbon element) caused by the Cottrell atmosphere was significantly related to the flow stress [11]. Thus, the slip band on the surface displaced after the ultimate rupture of DCI, as revealed by the atomic force microscopy (AFM) images of the specimens (Fig. 4). The undulate profiles of the specimens showed the presence of intrusions and extrusions, which corresponded to their plastic deformation. The extrusion peak showed fluctuations perpendicular to the stress axis, and the valley of intrusions, which were interrupted by the extrusions, was also observed in the plastic region.

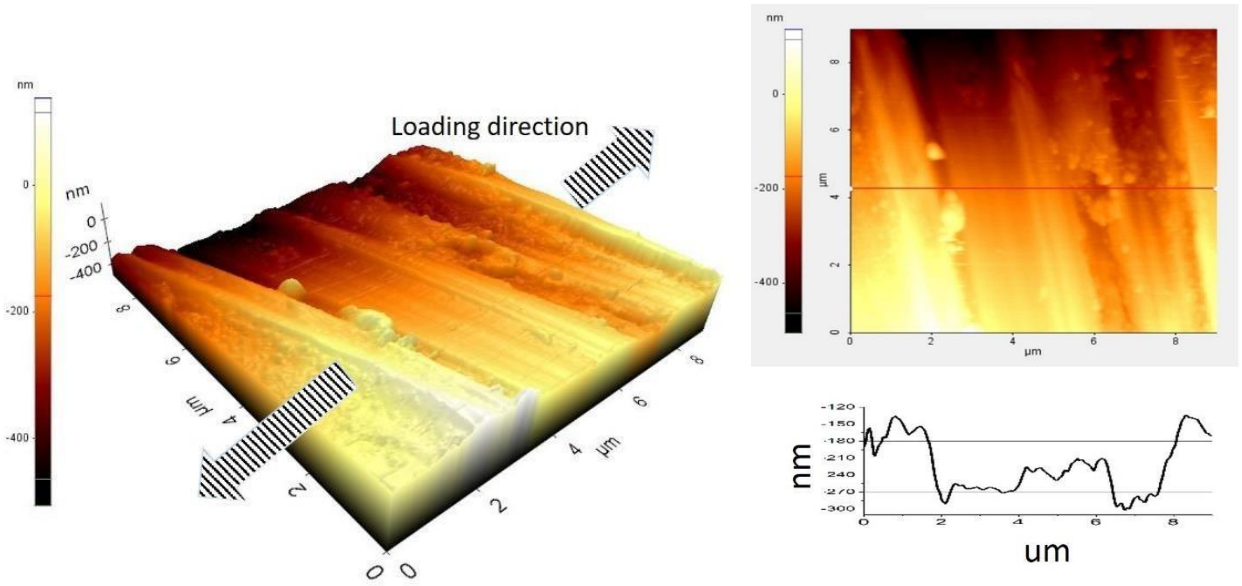

Figure 4. AFM topographic image of the surface deformed at −30 °C.

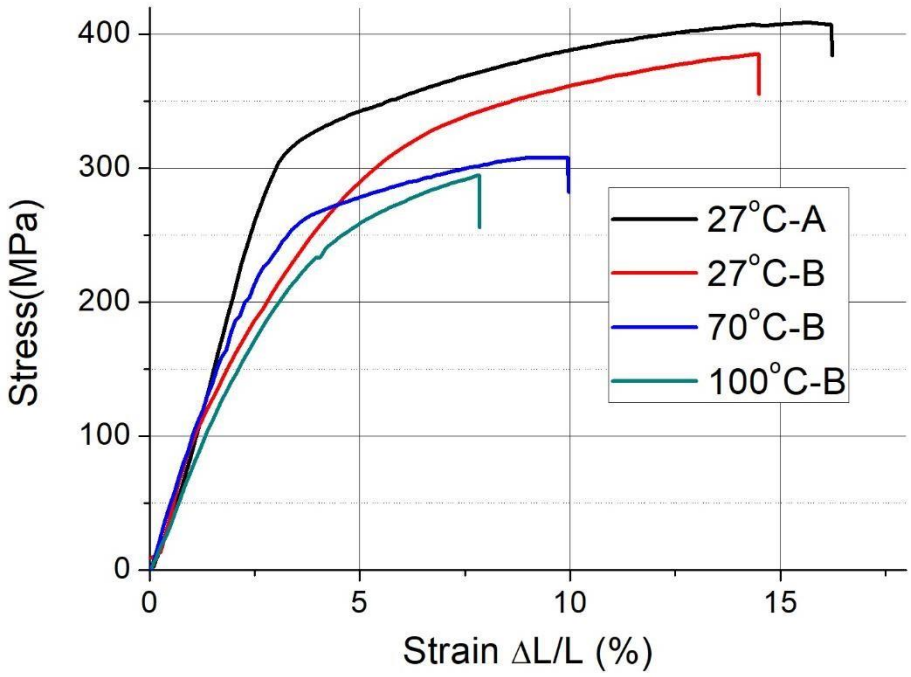

Figure 5. Tensile properties of the DCI specimens exposed to brine water at various temperatures. A: atmospheric condition, B: brine water (strain rate 2.5 x $10^{-5}$$sec^{-1}$).

Moreover, the SCC behavior of DCI was investigated by SSRT in brine water. The strain rates of the DCI specimens at 100, 70, and 27 °C were 7.8%, 9.9%, and 14.5%, respectively. As can be observed from Table 2, the elongation rate of the specimens decreased with an increase in the operational temperature. The local stress accumulation due to corrosion resulted in a minor deformation in the specimens. The DCI specimens showed brittleness because of presence of Cl^- and were susceptible to brine water. The rigorous corrosion in brine water predominated the brittle fracture of the DCI specimens, as shown in Fig. 5.

3.2. Fracture surface analysis

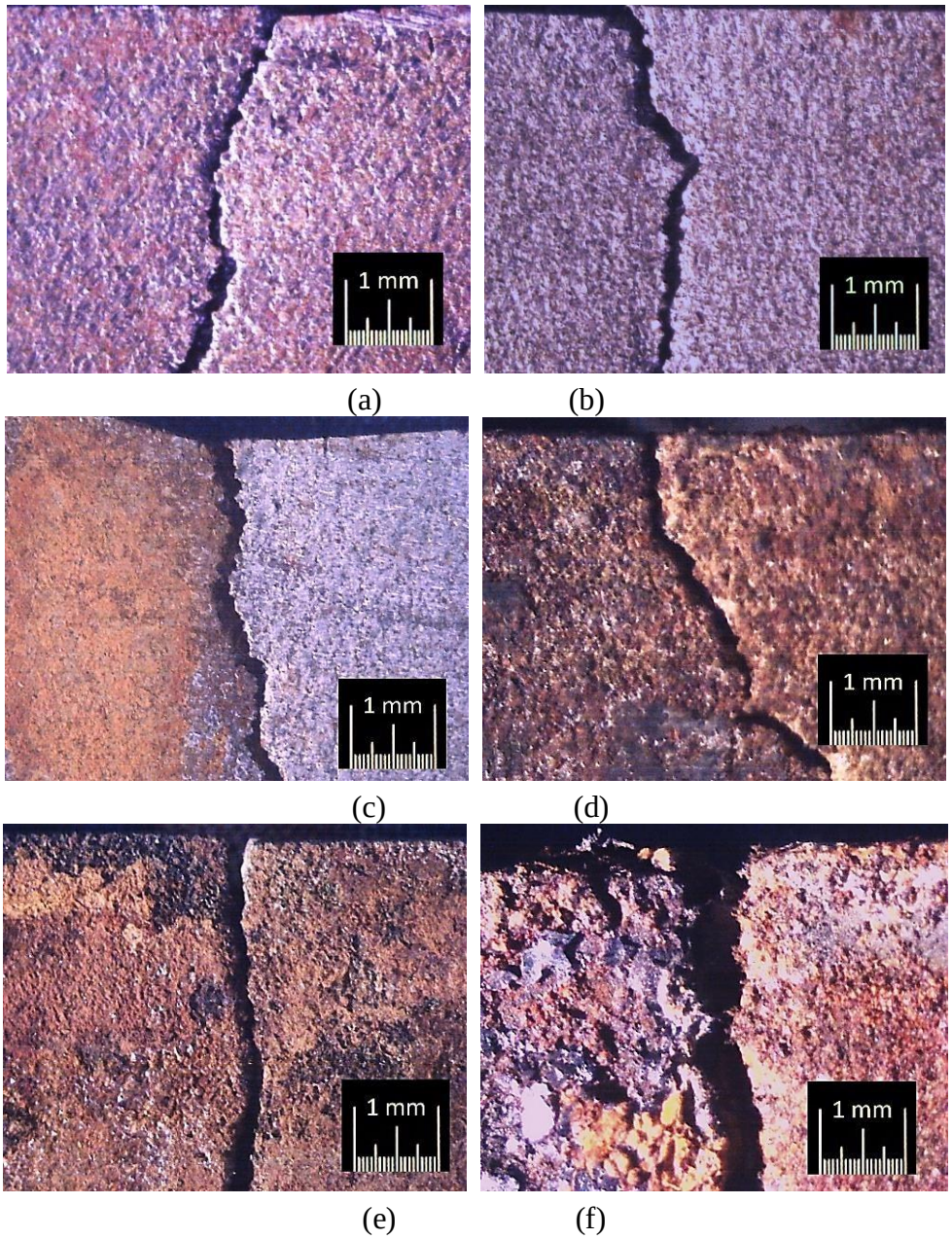

Figure 6. Optical images of the DCI specimens after SSRT (strain rate 2.5 x $10^{-5}$$sec^{-1}$) at (a) 100, (b) 27, (c) −30, (d) 27, (e) 70, (f) 100 °C; (a)–(c) atmospheric condition and (d)−(f) brine water.

Optical microscopy was employed to observe the morphology of the fracture surfaces of the specimens, and the irregular curve demonstrated as the lateral view of fractography (Fig. 6). Significant plastic deformation was caused by the energy absorption prior to the fracture of the specimens, as shown in Fig. 6 (c). The mechanical properties of the specimens corresponded to their crack propagation in the fracture zone, as mentioned in section 3.1. However, the toughness of the DCI specimens increased in the subfreezing environment. The corrosion behavior of DCI in the presence of the Cl^- ions of brine water. Moreover, the corrosion of the DCI specimens in brine water was investigated by obtaining their Cl^- kinetics, especially at high temperatures. Therefore, minor plastic deformation was caused by SSC and the smooth arc perpendicular to the applied stress (Figs. 6 (c–e)). It was found that the mechanical properties of the specimens deteriorated in the brine water environment, especially at high temperatures.

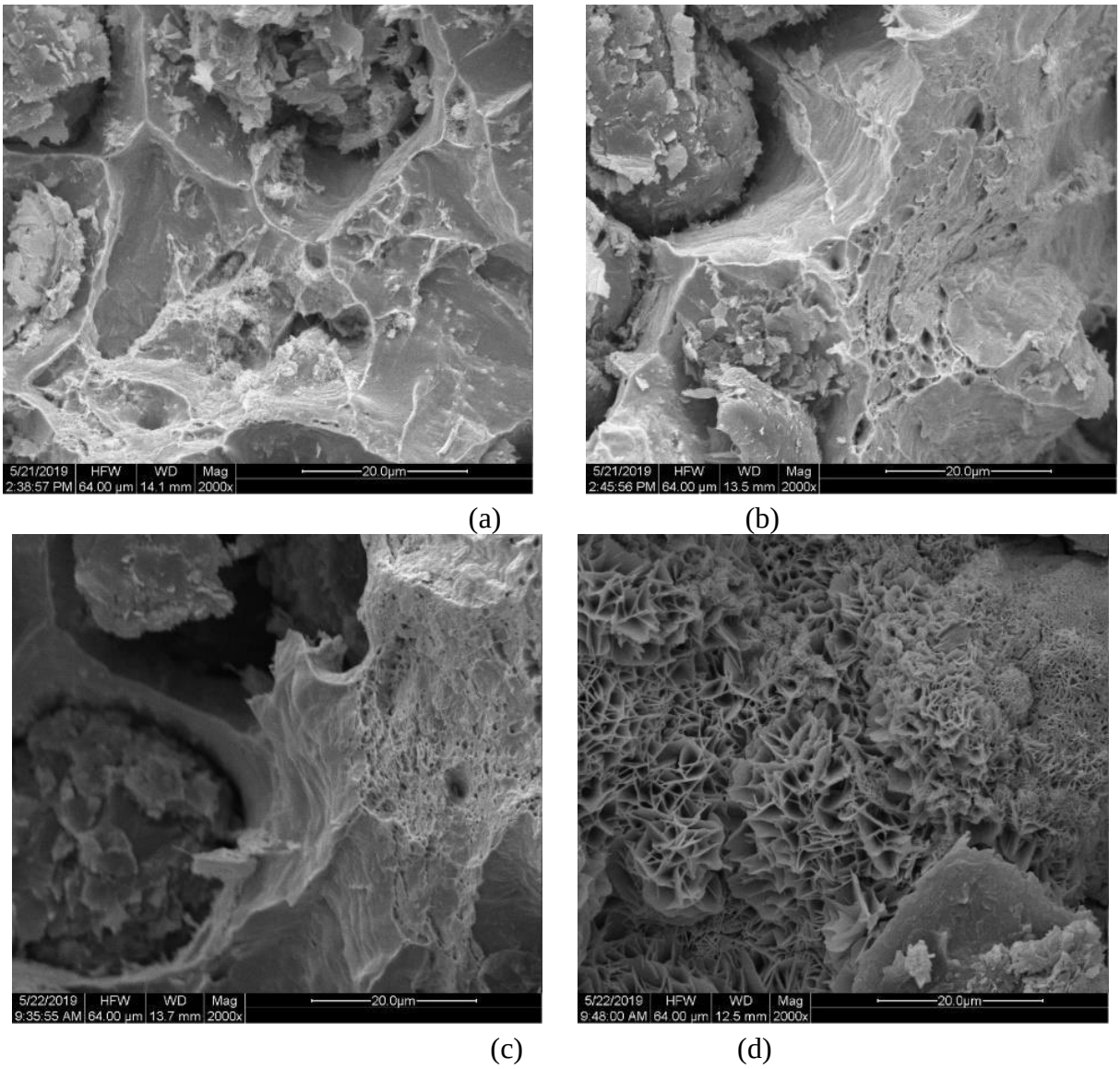

Figure 7. SEM images of the fracture surfaces of the specimens after SSRT (strain rate 2.5 x 10^{-5}sec^{-1}) at (a) 100 (b) 27 (c) −10 °C in ambient environment, (d) 70 °C in 3.5 wt% brine water.

The scanning electron microscopy (SEM) images of the specimens showed the occurrence of dimpled rupture fracture (Fig. 7). The specimens showed the characteristics of brittle-type cleavage fracture in brine water and partial ductile fracture due to quasi-cleavage features in the ambient environment [12-13]. The formation and coalescence of dimples (vacancies) accompanied the propagation of a cleavage crack, especially in the subfreezing condition (Fig. 7 (a–c)), indicating the presence of ductile cracks in the specimens [8,14]. A needle-shaped oxide substance appeared on the ruptured surface of the specimens after SSRT [15]. This can be attributed to the corrosion of the ferrite phase and the disappearance of a small graphite nodularity in the matrix (Fig. 7(d)).

3.3. Corrosion rate

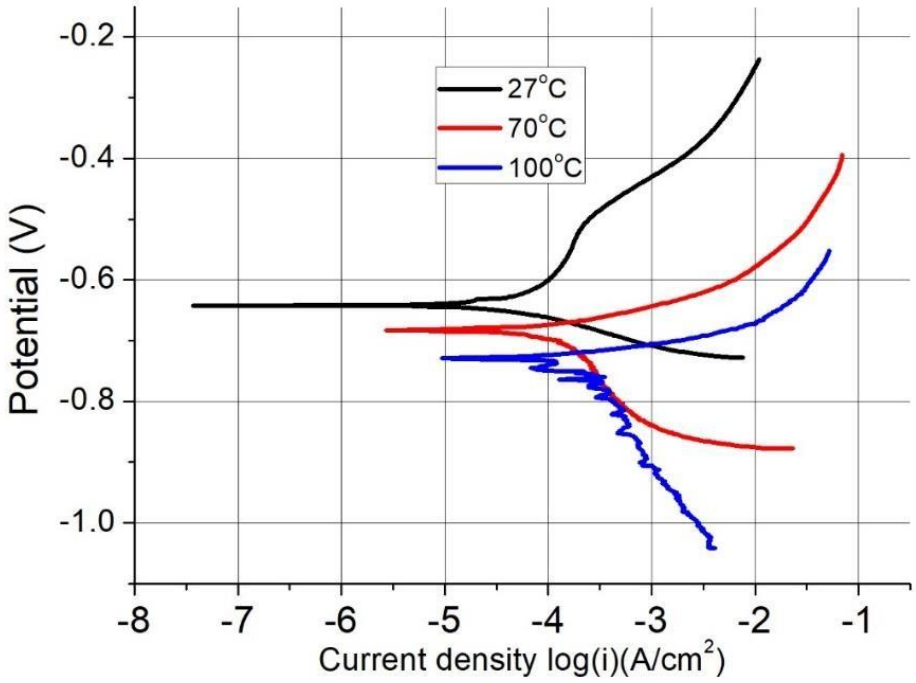

Figure 8. Potentiodynamic polarization curves of the specimens in brine water (sweeping potential from −1.1 to 0.2 V).

.

The migration rate of Cl^- ions predominated the chemical kinetics of the specimens, and their free energy decreased with an increase in the temperature of the liquid. Hence, the Cl^- ions penetrated the oxide film of DCI, causing pitting corrosion on its surface. The potentiodynamic polarization curves of the DCI specimens were obtained under simulated environments (3.5 wt% NaCl). From Fig. 8, it can be observed that the corrosion current densities of the specimens at 100, 70, and 27 °C were 3.84×10^{-4}, 8.97×10^{-5}, and 3.97×10^{-5} A/cm^2, respectively. The corrosion rate of DCI under the ambient condition was more than one order of magnitude lower than that under the extreme condition [6,16]. The experimental results indicated that the corrosion resistance of the passive film on the DCI specimens abruptly decreased with an increase in temperature [17].

OCP test was also carried out to investigate the stability of the oxide films on the specimens [18]. The OCP of the specimens shifted negatively with an increase in temperature.

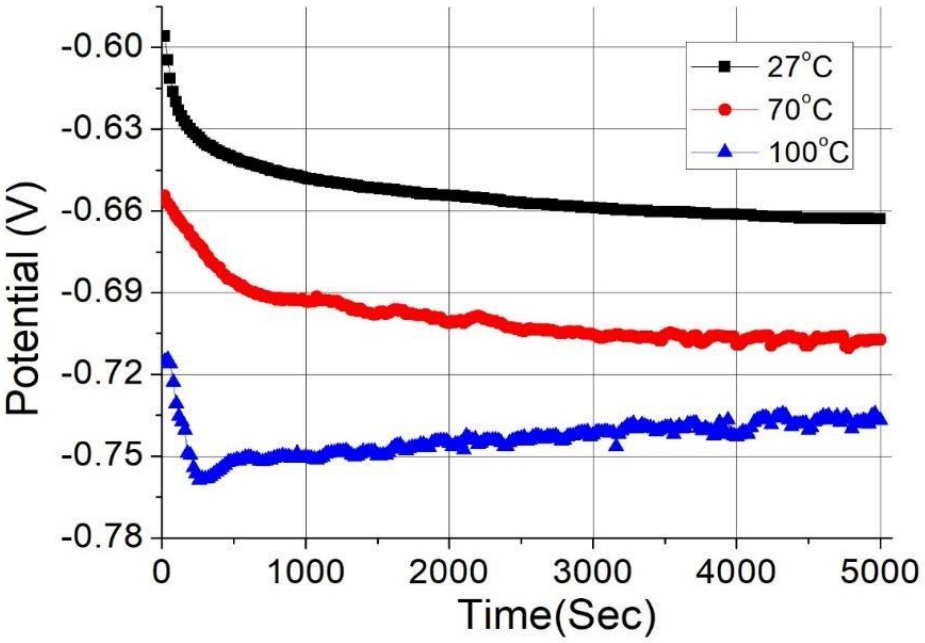

Figure 9. OCP test at different temperatures in brine water.

Meanwhile, the changes in the potential of the specimens with time were recorded (Fig. 9). The potentials of the specimens treated at 100 and 70 °C showed significant fluctuations with time. The specimen treated at 27 °C asymptotically approached −0.66 V and existed in the metastable state. This result indicates that the stability of the specimens was significantly affected by the passive films on their surfaces, and the thickness of the film varied with time during the electrochemical reaction [19].

4. CONCLUSION

The effects of thermal treatment conditions and brine water exposure on the mechanical properties of DCI were investigated. The failure behavior of DCI was significantly influenced by the thermal treatment and exposure conditions. Moreover, the DCI specimens treated at

100, 27, and −30 °C showed tensile strengths of 388.8, 408.5, and 440.2 MPa, respectively. The toughness of the DCI specimens corresponded to the existence of dimples on their fracture surfaces. Furthermore, DCI showed a ductile behavior and the existence of slip bands in the subfreezing environment (−30 °C), as revealed by the AFM images. The corrosion currents of the specimens treated at 100 and 27 °C were 3.84×10^{-4} and 3.97×10^{-5} A/cm^2, respectively. At the ambient temperature, DCI was protected by a metastable oxide film in brine water (3.5 wt% NaCl), and the OCP shifted negatively with an increase in temperature. The severe corrosion of DCI was responsible for the specimen failure in brine water, particularly in boiled water. DCI exhibited brittle properties because of the existence of Cl^- and was susceptible to brine water. Further research is required to investigate the effect of

atmospheric pollutants (such as sulphur oxides and nitrogen oxides) on the properties DCI in liquid environments.

ACKNOWLEDGEMENTS
The authors acknowledge material support provided by the Kuo Toong International Co., LTD. of the Republic of China.

References

1. J.l. Wang, Y. Wu, J. Liu, *Int. J. Electrochem. Sci.,* 8 (2013) 4631.
2. N. Zapp, O. Weber, H. Natter, *J. Electrochem. Sci.,* 10 (2015) 5434.
3. H. Zhang, Y. Tian, H. Guo, M. Kang, Y. Song, *J. Electrochem. Sci.*, 13 (2018) 9069.
4. R.K. Singh Raman, B.C. Muddle, *Mater. Sci. Technol.*,19 (2003) 1751.
5. M. Cavallini, O.D. Bartolomeo, F. Iacoviello, *Eng. Fract. Mech.,* 75 (2008) 694.
6. C.H. Hsu, M.L. Chen, *Corr. Sci*., 52 (2010) 2945.
7. R.A. Martínez, *Eng. Fract. Mech.*, 77 (2010) 2749.
8. Y. Sun, S. Hu, Z. Xiao, S. You, J. Zhao, Y. Lv, *Mater. Des.*, 41 (2012) 37.
9. H. Pancheva, *J. Enterp. Technol.,* 4 (2017) 59.
10. R.A. Gonzaga, *Mater. Sci. Eng. A.,* 567 (2013) 1.
11. Y. Qiu, J.C. Pang, M.X. Zhang, C.L. Zou, S.X. Li, Z.F. Zhang, *Int. J. Fatigue.,* 12 (2018) 12.
12. A. Alhussein, M. Risbet, A. Bastien, J.P. Chobaut, D. Balloy, J. Favergeon, *Mater. Sci. Eng. A.,* 605 (2014) 222.
13. C. Fragassa, N. Radovic, A. Pavlovic, G. *Minak, Tribol. Ind.*, 38 (2016) 49.
14. Y. Qiu, J.C. Pang, S.X. Li, E.N. Yang, W.Q. Fu, M.X. Liang, Z.F. Zhang, *Mater. Sci. Eng. A.*, 664 (2016) 75.
15. Y. Song, Y. Tian, X. Zhao, H. Guo, H. Zhang, *J. Electrochem. Sci.,* 11 (2016) 7031.
16. D. Medyński, A. Janus, *Arch. Foundry. Eng.,* 16 (2016) 63.
17. C.S. Brandolt, M.A. Rosa, L.B. Ramos, R.M. Schroeder, C.F. Malfatti, I.L. Müller, *Mater. Sci. Technol.,* 33 (2017) 227.
18. H. Guo, Y. Tian, H. Shen, X. Liu, Y. Chen, *J. Electrochem. Sci.,* 11 (2016) 6993.
19. B. Qi, C. Cui, Y. Yuan, *J. Electrochem. Sci.,* 10 (2015) 545.